Resolution Enhanced Non-Contact Thermoacoustic Imaging using Coded Pulse Excitation

Ajay Singhvi, Aidan Fitzpatrick and Amin Arbabian
Department of Electrical Engineering, Stanford University, Stanford, CA, USA

***Abstract*—Non-contact thermoacoustic and photoacoustic imaging systems which combine the high resolution of ultrasound with good dielectric/optical contrast show promise in many medical, remote sensing and non-destructive testing applications. One approach that enables meeting the challenging signal-to-noise constraints in non-contact imaging is the use of highly sensitive, resonant air-coupled capacitive micromachined ultrasound transducers (CMUT) as receivers. This sensitivity, however, is gained through a fundamental tradeoff with bandwidth and is at the cost of lower image quality due to slowly decaying residual oscillations of the underdamped, high quality factor CMUTs. In this paper, we propose a pulse-based, multi-cycle signal excitation scheme which optimally modulates the generated ultrasound pressure via the thermoacoustic effect so as to actively cancel the residual oscillations of the CMUT response. This improves achievable thermoacoustic image resolution and reduces multi-path clutter. The proposed technique can also be used to improve resolution in contact-based imaging systems that use resonant sensors.**

***Index Terms*—capacitive micromachined ultrasonic transducer, CMUT, coded excitation, microwave-induced thermoacoustics, non-contact, photoacoustics, resonant sensors**

I. Introduction

Hybrid sensing systems that rely on the microwave-induced thermoacoustic (TA) or photoacoustic (PA) effect are becoming increasingly prevalent for applications like biomedical imaging, non-destructive testing, and remote sensing and communications [1]–[3]. Such hybrid modalities take advantage of the dielectric or optical contrast offered by the electromagnetic (EM) excitation, while achieving good spatial resolution due to ultrasonic detection.

To make these modalities truly ubiquitous, research has focused on building portable, low-cost systems via the use of low-power integrated power amplifiers [4] and laser diodes [5] albeit at the cost of a lower signal-to-noise ratio (SNR). Additionally, like conventional ultrasound (US) systems, these TA/PA systems often use a coupling gel to establish direct contact with the sample – producing images that are operator-dependent and making it difficult to use in applications where contact is infeasible. Non-contact thermoacoustic and photoacoustic systems (NCTA) shown schematically in Fig. 1 have been proposed to overcome these limitations, but they too face a stringent SNR challenge [2], [6]. This is due to a large acoustic impedance mismatch at the sample-air interface,

This work was supported in part by Advanced Research Projects Agency-Energy Grant DE-AR0000825 and in part by the U. S. Office of Naval Research under award number N00014-19-1-2241. The authors would also like to thank Texas Instruments for equipment donations.

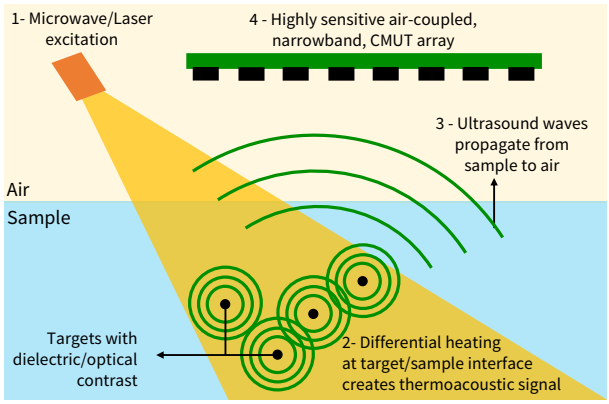

Fig. 1. Schematic representation of non-contact thermoacoustic and photoacoustic sensing systems using CMUT based detection.

resulting in significant signal attenuation as the US waves travel from the sample to air.

The signal strength challenge in such compact, low-power or non-contact versions of a TA system could be solved by using highly sensitive US receivers. Prior work [2] has utilized narrowband, resonant capacitive micromachined ultrasound transducers (CMUT) due to their high sensitivity and ease-of-integration with supporting electronics. However, the design of these CMUTs has an inherent tradeoff between device sensitivity and bandwidth – wherein one can obtain better SNR at the expense of a worse imaging resolution. A high quality factor (Q) resonant sensor requires multiple excitation cycles to ring up to sufficient sensitivity and has an underdamped response with slowly decaying oscillations. Both of these factors contribute to a longer sensor response duration which directly impacts image quality – lowering image resolution and creating undesired image artifacts.

Previously, coded excitation schemes have been proposed for resonant RF and US communication systems [7], [8] wherein a single excitation cycle is followed by an out-of-phase suppression cycle to cancel the residual oscillations, thereby enabling higher data rates. In a similar vein, this work develops a coded excitation scheme that enhances image resolution in hybrid TA systems by encoding the TA effect to suppress the residual oscillations. Moreover, we develop the scheme to account for a multi-cycle excitation since that is necessary to fully utilize the sensitivity of the resonant sensors used in low-power or non-contact systems. Significant improvement in image quality when using the proposed scheme for imaging complex scenes is also demonstrated.

978-1-7281-5448-0/20/$31.00 ©2020 IEEE

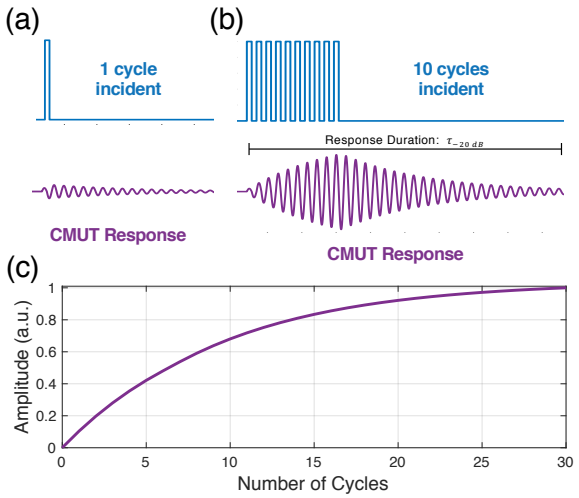

Fig. 2. (a) Typical one-cycle excitation (top) and corresponding CMUT response (bottom); (b) multi-cycle excitation (top) and corresponding CMUT response (bottom); (c) CMUT response amplitude dependence on number of excitation cycles

II. System Overview

A. Thermoacoustic Physics

To enable non-contact imaging as proposed in Fig. 1, an EM source in the form of a microwave source or laser can be used to stimulate US pressure waves via the TA effect at interfaces with dielectric/optical contrast. The creation and propagation of the US waves is governed by the TA wave equation:

$$\left(\nabla^2 - \frac{1}{v_s^2}\frac{\partial^2}{\partial t^2}\right) p(\boldsymbol{r},t) = -\frac{\beta}{C}\frac{\partial H(\boldsymbol{r},t)}{\partial t}, \tag{1}$$

where v_s is the speed of sound, $p(\boldsymbol{r},t)$ is the generated pressure at position $\boldsymbol{r}$ and time t, β is the thermal expansion coefficient, and C is the specific heat capacity. The heating function $H(\boldsymbol{r},t)$ quantifies the EM power absorbed per unit time and unit volume at position $\boldsymbol{r}$.

Strategically encoding the envelope of the EM power thus enables, via the TA effect, the creation of US waves that can be manipulated in a manner similar to single-modality coded excitation schemes [4].

B. Air-Coupled CMUT Receiver

Commonly in contact-based TA and US imaging systems, wideband sensors are used to achieve good imaging resolution. For non-contact systems, SNR challenges suggest the use of high-Q resonant sensors such as narrowband, air-coupled CMUTs that offer higher sensitivity than their wideband counterparts.

The CMUT discussed herein has been previously reported and has an experimentally measured minimum detectable pressure of 278 μPa_{RMS}. The CMUT has a center frequency (f_c) of 71 kHz and about 2.5 kHz of bandwidth – corresponding to a Q-factor of 28 [2]. Using these device characteristics, the CMUT can be modeled as a second-order pressure-to-voltage transfer function with the following frequency response:

$$G(\omega) = \frac{j\omega\omega_c/Q}{\omega_c^2 - \omega^2 + j\omega\omega_c/Q}, \tag{2}$$

where $\omega_c = 2\pi f_c$.

The high-Q of this CMUT, while advantageous for high sensitivity US detection, results in resonant behavior that adversely impacts imaging resolution. As seen in Fig. 2, the CMUT requires multiple cycles at its resonance frequency in order for its response to ring up to high amplitudes. Using multiple cycles is consequently fundamental to exploiting the high sensitivity of the CMUT; however, the more cycles that are used, the longer the CMUT response becomes.

In addition, the CMUT response in Fig. 2(b), shows that after the incident cycles end, there is a long decaying residual tail that is due to the continued oscillation of the high-Q CMUT plate. This long tail further extends the CMUT response duration and can obstruct subsequently received signals, thus equating to reduction in resolution in an imaging system. To capture the benefits of increased SNR while maintaining reasonable imaging resolution, it becomes critical to suppress the residual tail of the CMUT response.

To terminate the undesired residual oscillations of the CMUT plate and reduce the CMUT response duration, we propose the coded pulse excitation scheme described in the next section.

III. Coded Pulse-Excitation

Intuitively, in order to suppress the undesired residual oscillations of the CMUT plate one could impinge the plate with additional US waves tailored to counteract the originally induced oscillations, bring the plate back to equilibrium, and reduce the CMUT response duration. These US waves generated to inhibit the oscillations should satisfy two conditions to ensure efficient suppression: (i) **precise timing**, so that they are out-of-phase with the oscillations that were originally excited and (ii) **appropriate amplitude** to ensure that they can counteract the undesired residual oscillations.

As a representative example to explain the proposed scheme, we begin with a case of 2 excitation cycles, different scenarios for which are illustrated in Fig. 3(a)-(h). Throughout the figure, excitation cycles and responses are seen in blue, suppression cycles and responses in red, and composite cycles and responses in purple. Note that due to peak power limitations imposed by the EM source, the maximum source amplitude is fixed and normalized to 1 in all scenarios.

In the first scenario shown in Fig. 3(a), we have 2 excitation cycles with amplitude A_e followed by a single, appropriately time-shifted suppression cycle with amplitude $A_s > A_e$. This creates a composite response in Fig. 3(d), with the residual tail suppressed due to the excitation and suppression responses being exactly out-of-sync. On the other hand, we could also introduce 2 appropriately time-shifted suppression cycles with amplitudes $A_s < A_e$ as shown in Fig. 3(e). This provides similar suppression as seen in Fig. 3(h). There are tradeoffs involved in the two scenarios: the coded excitation in Fig. 3(c) provides the fastest suppression but with lower response amplitude (Fig. 3(d)) while the coded excitation in Fig. 3(g) results in higher response amplitude at the cost of a slightly delayed suppression (Fig. 3(h)).

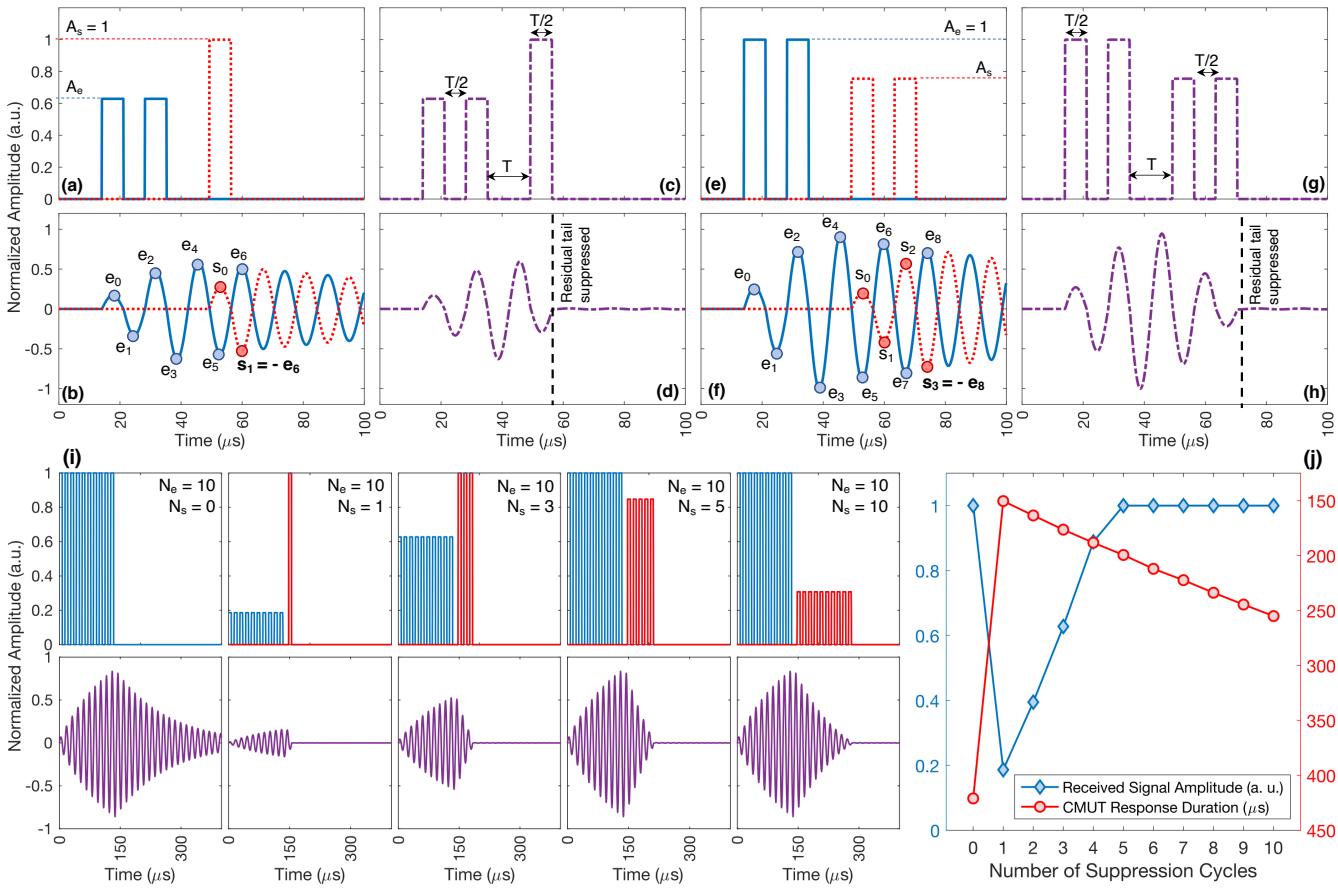

Fig. 3. (a) 2 excitation cycles (in blue) and one suppression cycle (in red) with amplitude $A_s > A_e$; (b) CMUT response to the cycles in (a); (c),(d) composite cycles and CMUT response from (a),(b); (e) 2 excitation cycles (in blue) and two suppression cycles (in red) with amplitude $A_s < A_e$; (f) CMUT response to the cycles in (e); (g),(h) composite cycles and CMUT response from (e),(f); (i) coded excitation scheme (top) and corresponding CMUT response (bottom) for a 10 cycle $(N_e = 10)$ excitation and varying the number of suppression cycles (N_s); (j) tradeoff in received signal amplitude and CMUT response duration for the case with $N_e = 10$ and varying N_s

The heuristic followed in the 2 cycle example above can be codified to apply to a more generic scenario with N_e excitation cycles and N_s suppression cycles. The suppression cycles need to be tailored such that the time-shift T_s between the set of excitation and suppression cycles is:

$$T_s = \frac{n}{f_c} \qquad (n = 1, 2, 3 \ ...), \tag{3}$$

However, to ensure quickest suppression and to meet energy constraints that the EM sources might impose, it is expeditious to choose $n = 1$ in the above equation. Assuming $n = 1$, the amplitude of the suppression cycles can be then scaled relative to the excitation cycles using a scaling factor k as follows:

$$A_s = kA_e \quad with \quad k = \frac{a_{N_e+N_s}}{a_{2N_s-1}}, \tag{4}$$

where a_x is the amplitude of the $(x+1)^{th}$ peak in the modeled CMUT response derived from (2). Inaccuracies in sensor modeling or deviations from the optimal time-shift and amplitude scaling would reduce the efficacy of the proposed scheme though minor differences would still allow for significant suppression of the residual oscillations.

Using (3) and (4), we design optimal coding schemes for a more practical excitation scenario that uses 10 excitation cycles to get reasonable CMUT sensitivity. Its variation in response with a different number of tailored suppression cycles is shown in Fig. 3(i). Given the peak power limitation, too few suppression cycles results in degradation in SNR, while using too many (once $A_s < A_e$) provides no overt benefits. Thus, as seen in Fig. 3(j) there is a range of suppression cycles that provides a significant reduction in CMUT response duration while maintaining high signal amplitudes.

IV. Imaging Results

To demonstrate the efficacy of our proposed scheme in practical imaging applications, we employ it in our previously reported below-ground NCTA imaging system [9]. The system concept for this application is shown in Fig. 4(a). Root structures or other buried objects with dielectric contrast to soil can be excited by modulated microwave energy to generate TA signals. These pressure waves then propagate through the soil and across the soil-air interface and can be detected with our air-coupled CMUTs. Following post-processing, we can reconstruct an image of the below-ground objects.

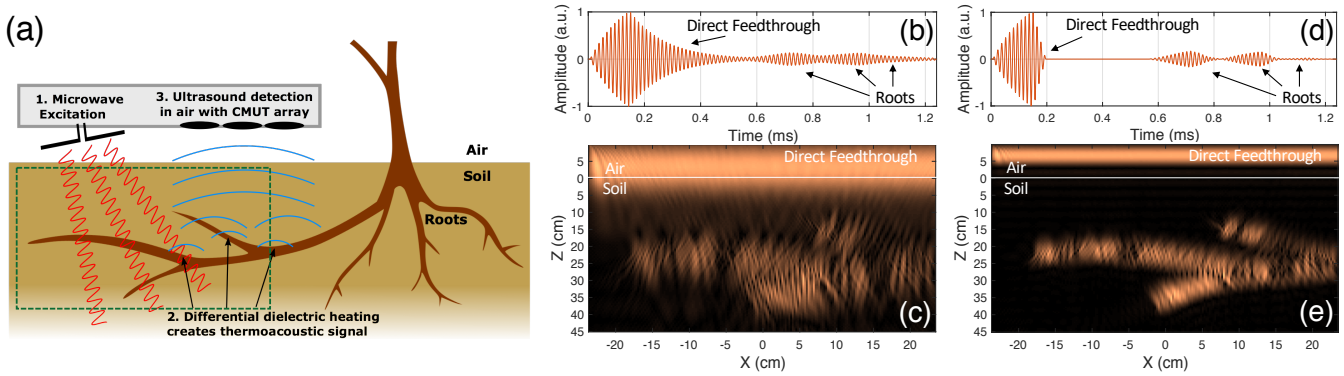

Fig. 4. (a) Concept of operation for a below-ground non-contact thermoacoustic imaging system; the roots in the dashed region are reconstructed in (b) reconstructed image of the roots without the proposed coded excitation scheme, showing multiple artifacts and poor image quality and (c) reconstructed image of the roots using the proposed coded excitation scheme, showing improved image quality

For the initial results presented in this paper, we test the proposed technique in simulation using the k-Wave toolbox in MATLAB [10]. In the simulation environment, we model the root structure shown in the enclosed dashed region of Fig. 4(a) as a collection of TA sources. Our previous work [2] in which we begin with a full EM simulation validates the use of this simplified modeling. The speed-of-sound in soil and air have been chosen as 500 m/s and 340 m/s, respectively [11]. The CMUTs have been modeled as a 50 cm array of point detectors with half-wavelength spacing that are located 10 cm above the soil-air interface. To incorporate the CMUT response, we perform a convolution of the final simulation data with the impulse response that corresponds to the CMUT transfer function in (2). Finally, we include TA point sources at each CMUT element location to model the direct feedthrough, or coupling, of the microwave energy to the CMUT receivers.

We perform two simulations with the setup described above. The TA signal in the first simulation is composed of 10 excitation and no suppression cycles. The reconstructed image for this case is shown in Fig. 4(c) and has poor resolution. This is due to the signal-of-interest being obscured by the elongated CMUT response to multiple TA signals and direct feedthrough, as shown in a representative A-scan in Fig. 4(b). The second simulation has a TA signal that is comprised of 10 excitation and 3 properly scaled suppression cycles using the heuristic described in Section III. For this simulation, the A-scan data as seen in Fig. 4(d) is visibly cleaner, with multiple TA signals clearly delineated. The reconstructed image in Fig. 4(e) thus shows not only improved resolution and image quality with high-fidelity reconstruction of the roots, but also significant reduction of the direct feedthrough signal that may have obscured shallow targets in Fig. 4(c).

V. Conclusion

In this paper, we present a coded pulse excitation scheme which enables improved resolution when using highly resonant US sensors in applications where sensitivity is critical. The heuristic provided within can be generalized to any resonant sensor to suppress slowly decaying residual oscillations. While this requires an analytical model of the sensor, even crude modeling can provide significant suppression of undesired resonant behavior, reduce the response duration, and thereby enhance image resolution. Future work will quantify the amount of suppression achieved with model inaccuracies, practical constraints, and experimental non-idealities. We have recently begun using this technique successfully in experimental work for both microwave-induced thermoacoustic and photoacoustic systems, which we will also report on in future publications.

References

[1] F. Gao, X. Feng, and Y. Zheng, "Advanced photoacoustic and thermoacoustic sensing and imaging beyond pulsed absorption contrast," *Journal of Optics*, vol. 18, no. 7, p. 074006, 2016.

[2] A. Singhvi, K. C. Boyle, M. Fallahpour, B. T. Khuri-Yakub, and A. Arbabian, "A microwave-induced thermoacoustic imaging system with non-contact ultrasound detection," *IEEE transactions on ultrasonics, ferroelectrics, and frequency control*, vol. 66, no. 10, pp. 1587–1599, 2019.

[3] X. Wang, T. Qin, Y. Qin, R. S. Witte, and H. Xin, "Microwave-induced thermoacoustic communications," *IEEE Transactions on Microwave Theory and Techniques*, vol. 65, no. 9, pp. 3369–3378, 2017.

[4] H. Nan and A. Arbabian, "Peak-power-limited frequency-domain microwave-induced thermoacoustic imaging for handheld diagnostic and screening tools," *IEEE Transactions on Microwave Theory and Techniques*, vol. 65, no. 7, pp. 2607–2616, 2017.

[5] M. N. Cherkashin, C. Brenner, and M. R. Hofmann, "Transducer-matched multipulse excitation for signal-to-noise ratio improvement in diode laser-based photoacoustic systems," *Journal of biomedical optics*, vol. 24, no. 4, p. 046001, 2019.

[6] G. Rousseau, A. Blouin, and J.-P. Monchalin, "Non-contact photoacoustic tomography and ultrasonography for tissue imaging," *Biomedical optics express*, vol. 3, no. 1, pp. 16–25, 2012.

[7] F. Inanlou, M. Kiani, and M. Ghovanloo, "A 10.2 mbps pulse harmonic modulation based transceiver for implantable medical devices," *IEEE journal of solid-state circuits*, vol. 46, no. 6, pp. 1296–1306, 2011.

[8] K. Keramatzadeh and A. M. Sodagar, "High-rate ultrasonic link for data telemetry to implantable biomedical microsystems using pulse excitation," in *2018 IEEE Life Sciences Conference (LSC)*. IEEE, 2018, pp. 17–20.

[9] A. Singhvi, B. Ma, J. D. Scharwies, J. R. Dinneny, B. T. Khuri-Yakub, and A. Arbabian, "Non-contact thermoacoustic sensing and characterization of plant root traits," in *2019 IEEE International Ultrasonics Symposium (IUS)*. IEEE, 2019, pp. 1992–1995.

[10] B. E. Treeby and B. T. Cox, "k-wave: Matlab toolbox for the simulation and reconstruction of photoacoustic wave fields," *Journal of biomedical optics*, vol. 15, no. 2, p. 021314, 2010.

[11] F. Adamo, G. Andria, F. Attivissimo, and N. Giaquinto, "An acoustic method for soil moisture measurement," *IEEE transactions on instrumentation and measurement*, vol. 53, no. 4, pp. 891–898, 2004.